Article

Regioselective Carbyne Transfer to Ring-Opening Alkyne Metathesis Initiators Gives Access to Telechelic Polymers

Stephen von Kugelgen, Renee Sifri, Donatela Bellone, and Felix R. Fischer

J. Am. Chem. Soc., **Just Accepted Manuscript** • Publication Date (Web): 17 May 2017

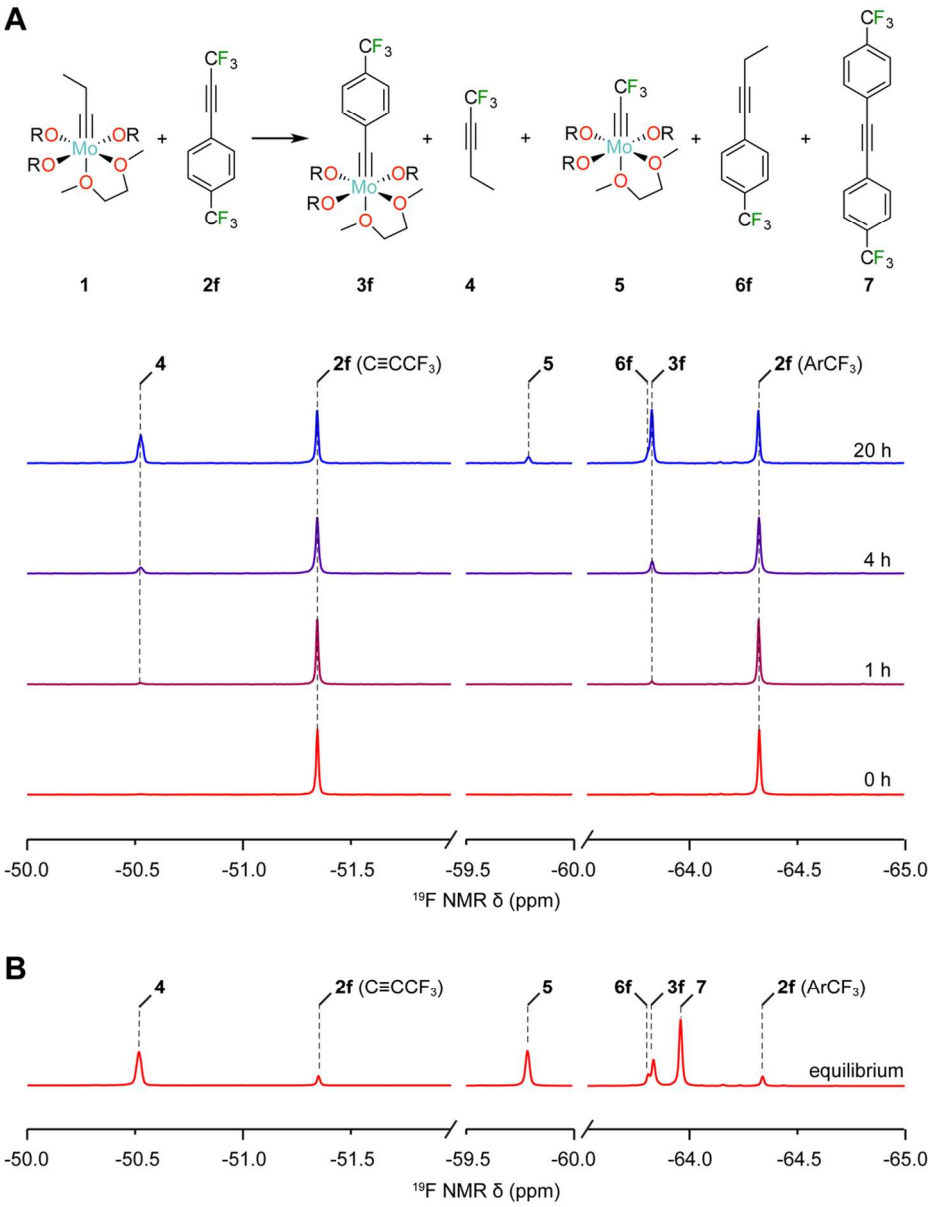

Figure 1

108x140mm (300 x 300 DPI)

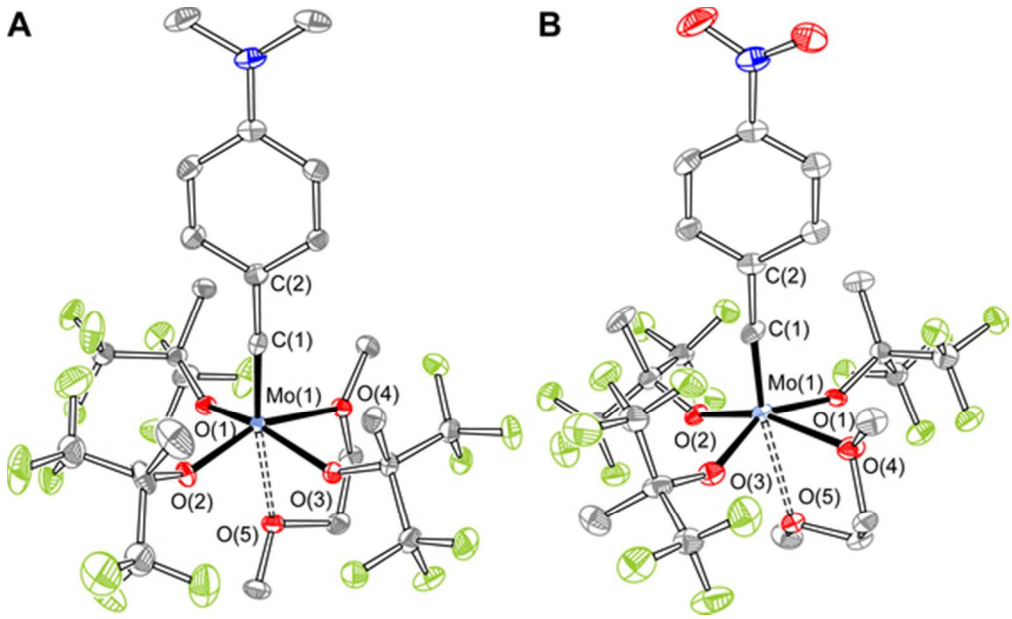

Figure 2

50x30mm (300 x 300 DPI)

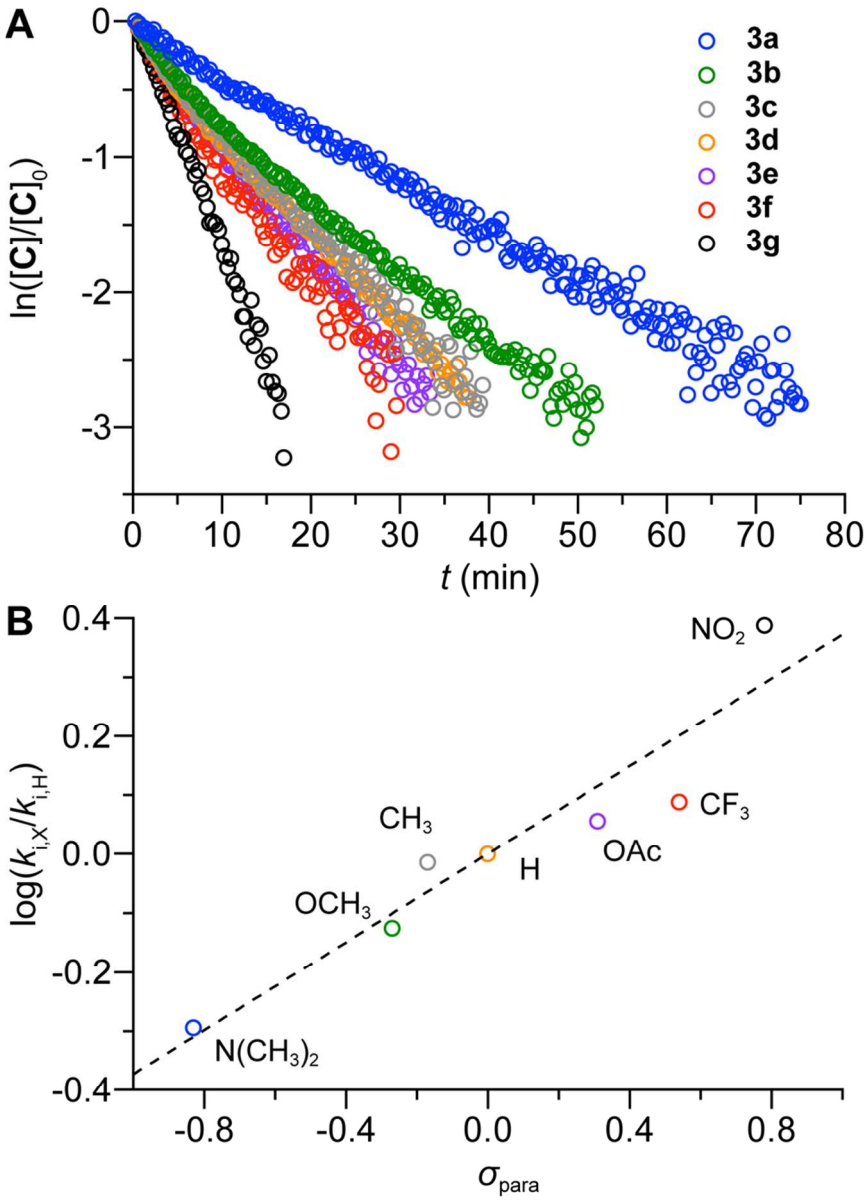

Figure 3

84x118mm (300 x 300 DPI)

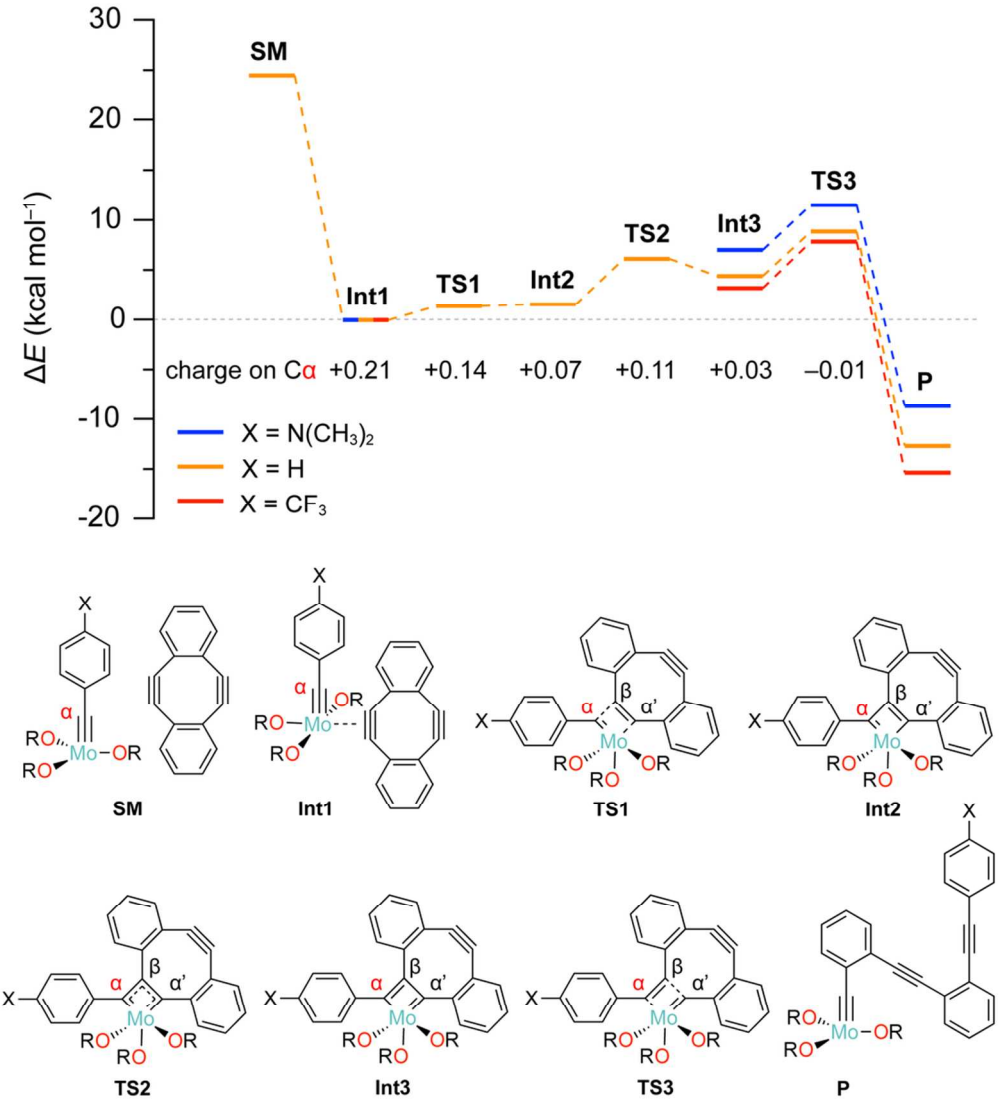

Figure 4

93x102mm (300 x 300 DPI)

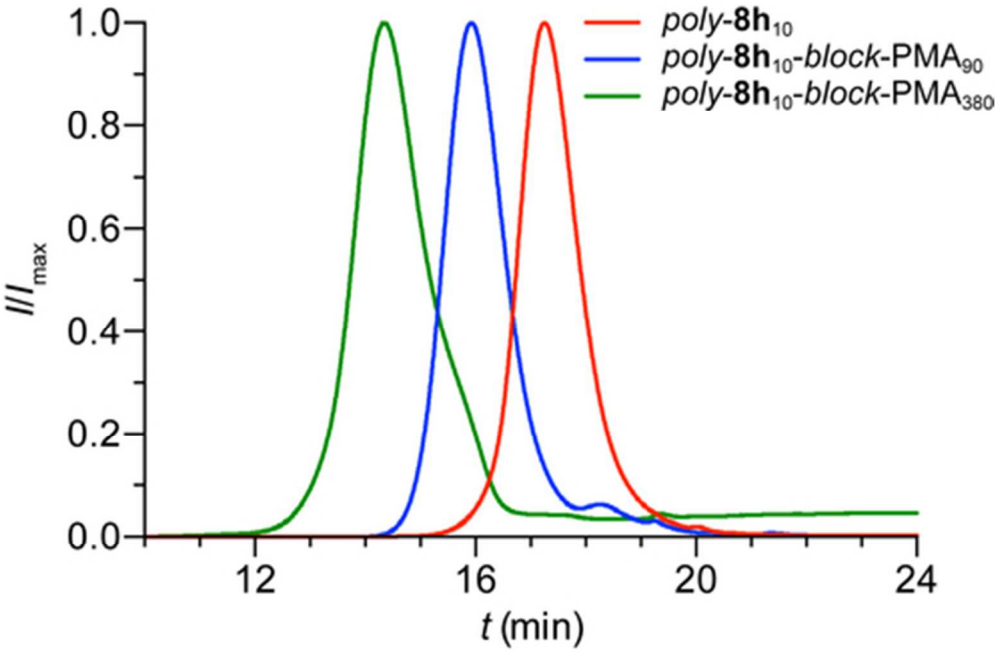

Figure 5

41x27mm (300 x 300 DPI)

previous work

low oxidation state route

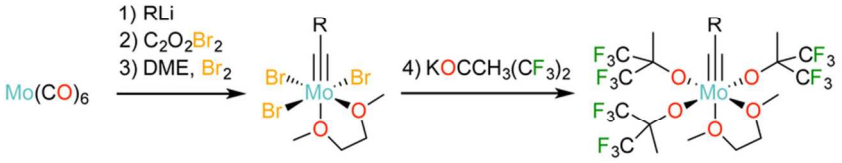

cross-metathesis route

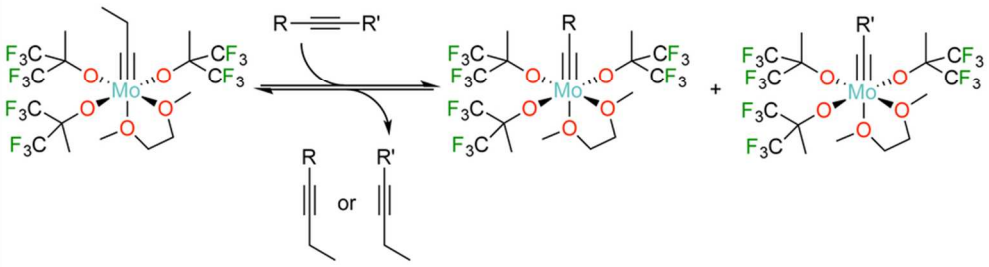

this work

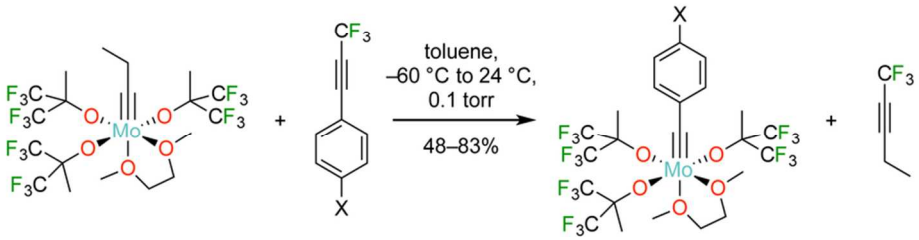

a, X = $N(CH_3)_2$; **b**, X = OCH_3; **c**, X = CH_3; **d**, X = H; **e**, X = OAc; **f**, X = CF_3; **g**, X = NO_2

Scheme 1

82x84mm (300 x 300 DPI)

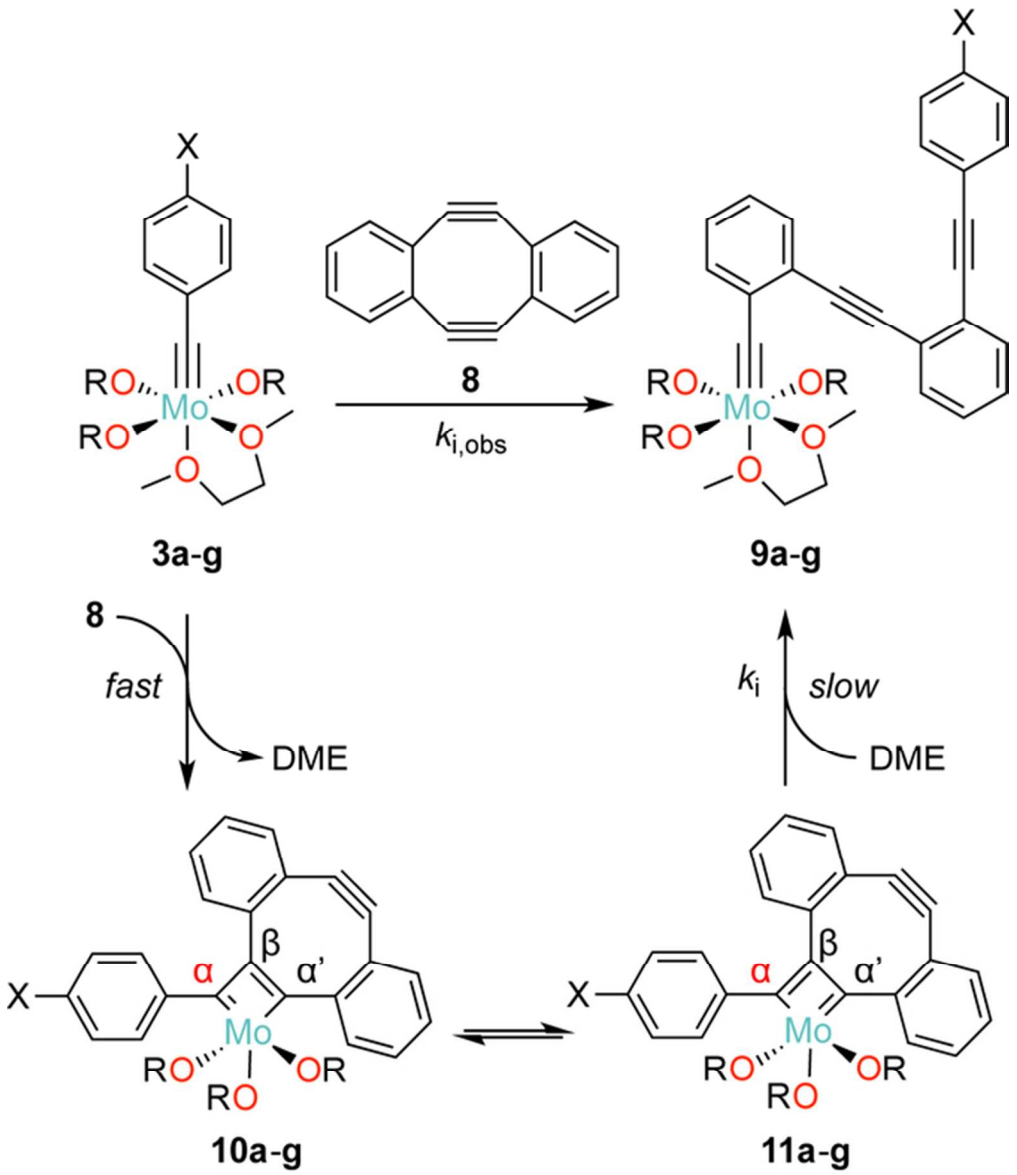

Scheme 2

56x66mm (300 x 300 DPI)

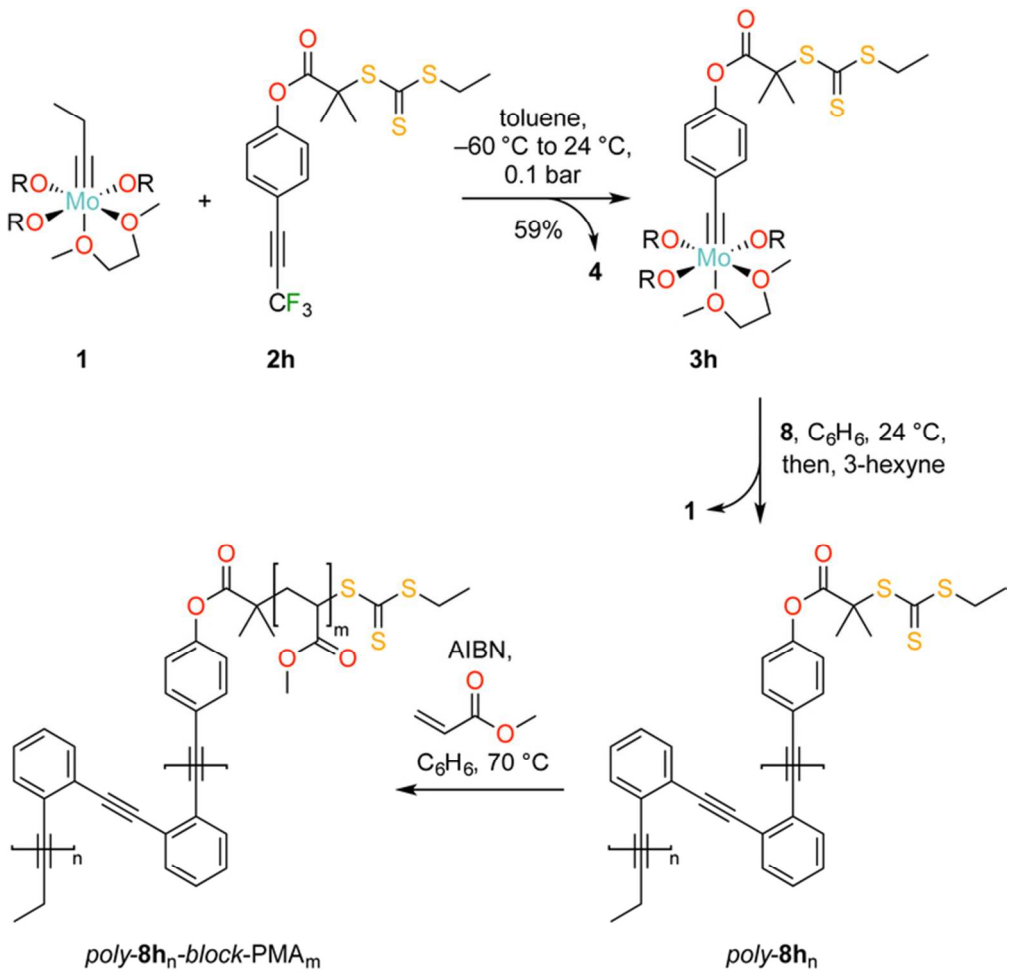

Scheme 3

66x63mm (300 x 300 DPI)

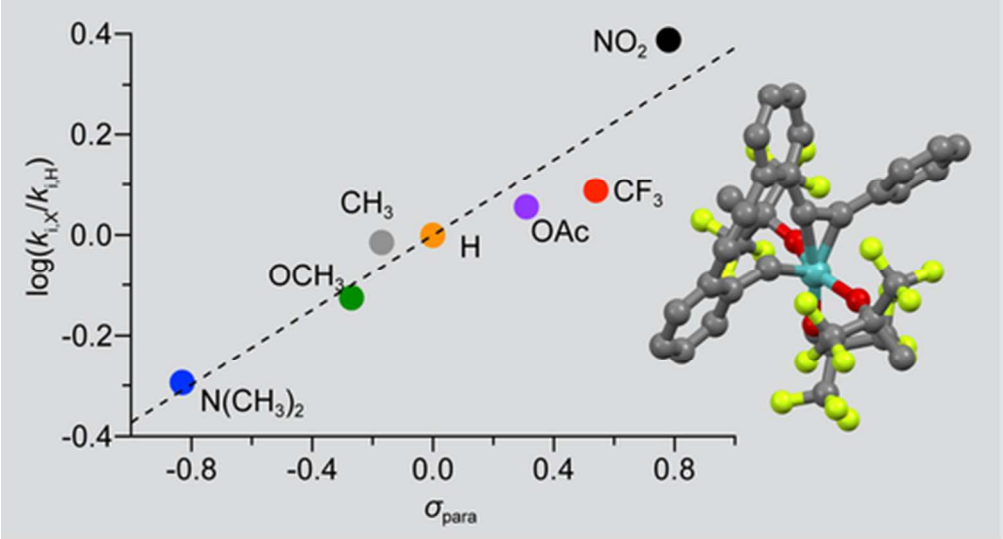

Table of Contents Image

44x23mm (300 x 300 DPI)

Regioselective Carbyne Transfer to Ring-Opening Alkyne Metathesis Initiators Gives Access to Telechelic Polymers

Stephen von Kugelgen,[†] Renee Sifri,[†] Donatela Bellone[†] and Felix R. Fischer[†∫||]*

[†]Department of Chemistry, University of California Berkeley, Berkeley, California 94720, United States

[∫]Materials Sciences Division, Lawrence Berkeley National Laboratory, Berkeley, California 94720, United States

[||]Kavli Energy Nanosciences Institute at the University of California Berkeley and Lawrence Berkeley National Laboratory, Berkeley, California 94720, United States

ABSTRACT: Regioselective carbyne transfer reagents derived from (3,3,3-trifluoroprop-1-yn-1-yl)benzene give access to functionalized ring-opening alkyne metathesis polymerization (ROAMP) initiators [R-$C_6H_4C{\equiv}Mo(OC(CH_3)(CF_3)_2)_3$] featuring electron-donating or withdrawing substituents on the benzylidyne. Kinetic studies and linear free-energy relationships reveal that the initiation step of the ring-opening alkyne metathesis polymerization of 5,6,11,12-tetradehydrobenzo[*a*,*e*][8]annulene exhibits a moderate positive Hammett reaction constant (ρ = +0.36). ROAMP catalysts featuring electron-withdrawing benzylidynes not only selectively increase the rate of initiation (k_i) over the rate of propagation (k_p) but also prevent undesired intra- and intermolecular chain transfer processes, giving access to linear *poly*-(*o*-phenylene ethynylene) with narrow molecular weight distribution. The regioselective carbyne transfer methodology and the detailed mechanistic insight enabled the design of a bifunctional ROAMP-reversible addition-fragmentation chain-transfer (RAFT) initiator complex. ROAMP followed by RAFT polymerization yields hybrid *poly*-(*o*-phenylene ethynylene)-*block*-*poly*-(methyl acrylate) block copolymers.

INTRODUCTION

Functional materials derived from semiconducting π-conjugated polymers have become ubiquitous in the field of organic electronics. A unique combination of rationally tunable band structures, favorable mechanical properties of polymers, and bulk solution-based synthesis and processing have contributed to the development of a wide variety of highly specialized functional materials for applications in organic light-emitting diodes (OLEDs),[1–3] organic photovoltaics (OPVs),[4–6] organic field effect transistors (OFETs),[7,8] and optical[9] and molecular sensors.[10] The performance of these polymers relies to a significant extent on the intra- and intermolecular interactions that span the gap between the nano- and the microscopic scale.[11–13] While the primary sequence of monomers largely determines the band gap and optical absorption, the preferred secondary structure adopted by polymer chains controls critical performance parameters like the mean free path of charge carriers and excitons.[14–18] Lastly, the challenge to direct the self-assembly of polymers into ordered microscopic domains, a tertiary structure, is a key technology in the fabrication of bulk heterojunctions for OPVs.[19–22] Herein we focus on conjugated polymers derived from *poly*-(phenylene ethynylene) (PPE) featuring a pattern of alternating aromatic rings and C≡C triple bonds. By varying the substitution pattern (*ortho*-, *meta*-, *para*-) along the aromatic rings lining the backbone of the polymer the secondary structure of PPEs can be adjusted from a linear zig-zag to a helically coiled conformation.[23–30] Classical syntheses of PPEs have relied on transition metal catalyzed cross-coupling or alkyne cross metathesis (ACM) step-growth polymerizations that suffer from unselective chain-termination, uncontrolled chain-transfer, and result in polymers with disproportionately broad molecular weight distributions.[31–37] We recently demonstrated the use of living ring-opening alkyne metathesis polymerization (ROAMP) of ring-strained cyclic alkynes with initiators derived from [$RC{\equiv}Mo(OC(CH_3)(CF_3)_2)_3$] for the controlled synthesis PPEs featuring either a linear or cyclic topology.[38]

In this study we report the first synthesis of telechelic PPEs by ROAMP using functional Mo carbyne initiators accessed by kinetically-controlled benzylidyne transfer to [$EtC{\equiv}Mo(OC(CF_3)_2CH_3)_3{\bullet}$DME] (**1**) (DME = 1,2-dimethoxyethane). Substituted (3,3,3-trifluoroprop-1-yn-1-yl)benzenes (**2**) serve as efficient carbyne transfer agents to yield substituted Mo benzylidynes [*p*-X-$C_6H_4C{\equiv}Mo(OC(CF_3)_2CH_3)_3{\bullet}$DME] (**3**). The mild conditions and high regioselectivity of this transfer protocol enable the incorporation of a wide range of functional groups into the structure of the ROAMP initiator. Linear free-energy relationship analysis reveals that the electronic structure of the ROAMP initiators controls the rate of initiation in the polymerization of 5,6,11,12-tetradehydrobenzo[*a*,*e*][8]annulene (**8**). A moderate positive Hammett reaction constant (ρ = +0.36) indicates that electron-withdrawing substituents stabilize a buildup of negative charge in the rate-determining transition state, a trend that is confirmed by theory. We demonstrate the versatility of our carbyne transfer protocol that provides access to well-defined PPE-*block*-*poly*-(methyl acrylate) (PMA) copolymers via reversible addition-fragmentation chain-transfer (RAFT)[39] chain extension of telechelic PPE macroinitiators derived from a bifunctional Mo ROAMP-RAFT initiator complex.

RESULTS AND DISCUSSION

Traditional routes toward substituted Mo benzylidyne complexes have thus far relied on the alkylation of $Mo(CO)_6$ with aryl lithium reagents followed by deoxygenation,[40–47] the cross-metathesis of $(RO)_3Mo{\equiv}Mo(OR)_3$ or $N{\equiv}Mo(OR)_3$ with symmetric/asymmetric arylethynes,[48–50] or the activation of trigonal planar $Mo(NRAr)_3$ complexes.[51–64] The harsh reaction conditions associated with low oxidation state routes[65] are incompatible with many polar functional groups. On the other hand, a cross-metathesis strategy suffers from low selectivity, unfavorable thermodynamic equilibria, and difficult purification of a complex product mixture. While the reversible cross-metathesis of Mo alkylidynes accessed by high oxidation state routes[66,67] e.g. $[EtC{\equiv}Mo(OC(CF_3)_2CH_3)_3 \bullet DME]$ (**1**) with symmetric 1,2-diarylethynes is facile, shifting the product mixture to the desired Mo benzylidyne complexes requires a large excess of reagent that proved challenging to separate by fractional crystallization. Cross-metathesis with asymmetric 1-aryl-1-alkynes such as 1-aryl-1-propynes instead leads to a mixture of Mo alkylidyne complexes (Supporting Information Figure S1) and the corresponding 1,2-diarylethyne. Our attempts to drive the reaction towards the desired product by either distilling or trapping the volatile 1,2-dialkylethyne with molecular sieves led to inseparable decomposition products.

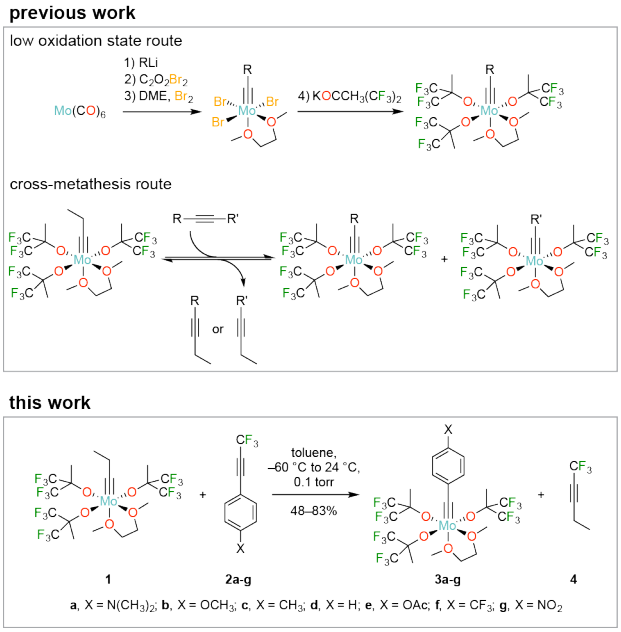

Scheme 1. Traditional low oxidation state and cross-metathesis routes toward substituted $[RC{\equiv}Mo(OC(CF_3)_2CH_3)_3{\bullet}DME]$ complexes (top). Schematic representation of the regioselective carbyne transfer with substituted (3,3,3-trifluoroprop-1-yn-1-yl)benzenes (**2a-g**) to give the corresponding molybdenum benzylidyne complexes (**3a-g**) (bottom).

To address this synthetic challenge, we developed a highly selective and functional group tolerant cross-metathesis protocol. The necessary requirements for an efficient carbyne transfer reagent are: i) high regioselectivity for the transfer of only the desired aryl group to the Mo complex; ii) side-products generated in the cross-metathesis step are either highly volatile or insoluble in the reaction mixture, facilitating the purification of the desired complex; and iii) the reaction conditions are mild and the carbyne transfer reagent is versatile enough to install a large variety of sensitive functional groups. Cross-metathesis of **1** with substituted (3,3,3-trifluoroprop-1-yn-1-yl)benzenes (**2a-g**) (Scheme 1) satisfies all three criteria. First, the electron withdrawing CF_3 group directs the regioselectivity of the cycloaddition to favor the transfer of the electron rich aromatic carbyne to the Mo metal center. Second, the fluorinated alkyne co-product, 1,1,1-trifluoropent-2-yne (**4**), is highly volatile, readily removed from the reaction mixture by application of a dynamic vacuum, and is electronically deactivated towards further metathesis when compared to unfluorinated 1,2-dialkylethynes. Finally, the cross-metathesis proceeds at mild temperatures ranging between –60 to 24 °C and is compatible with a wide variety of functional groups that cannot be introduced through a low-valent route. As an added bonus, characteristic shifts in the ^{19}F NMR signal associated with the CF_3 group in **2a-g** can serve as a highly sensitive internal reference for the progress of the reaction.

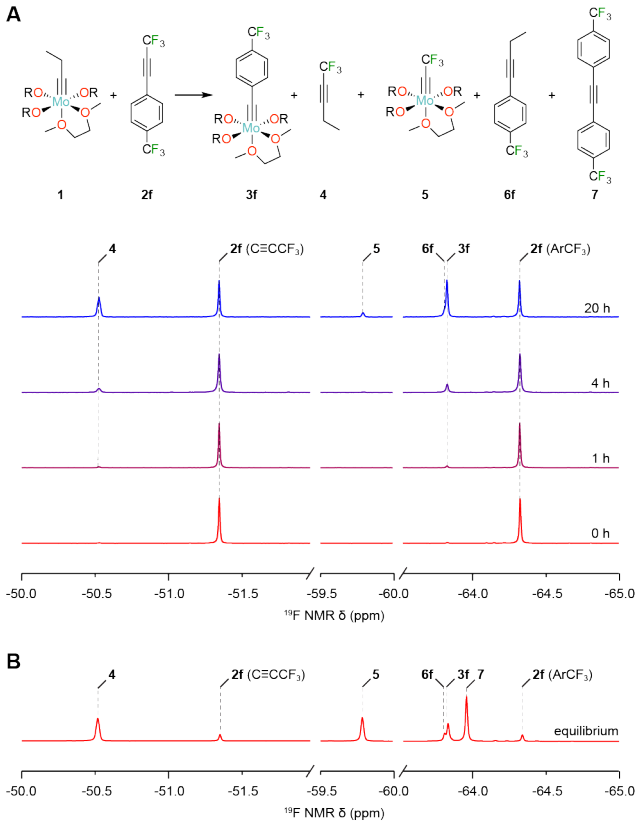

Figure 1. A) Time resolved ^{19}F NMR spectroscopy of the carbyne transfer of **2f** to **1** under kinetic control (–30 °C in $CDCl_3$, sealed NMR tube). B) ^{19}F NMR spectrum of the equilibrium mixture of the carbyne transfer reaction of **2f** to **1** under thermodynamic control (24 °C in $CDCl_3$, sealed NMR tube). R = $CCH_3(CF_3)_2$

The unusual regioselectivity inherent to our benzylidyne transfer reagents relies on the electron withdrawing CF_3 group in (3,3,3-trifluoroprop-1-yn-1-yl)benzenes (**2a-g**) that induces a polarization of the C≡C bond. The preferred orientation of the carbyne transfer reagent with respect to the Mo≡C bond in **1** places the electron-rich end of the C≡C bond bearing the substituted benzene ring next to the electron-deficient Mo center. Time resolved ^{19}F NMR spectroscopy (Figure 1A) reveals that under kinetic control (–30 °C, sealed NMR tube) the reaction of one equiv of **1** with 1-trifluoromethyl-4-(3,3,3-trifluoroprop-1-yn-1-yl)benzene (**2f**) leads predominantly to the formation of the desired trifluoromethylbenzylidyne complex **3f** over the undesired trifluoroethylidyne complex **5**. Based on the conservative assumption that the small amount of **5** present in the reaction mixture (Figure 1A, 20h)

is directly formed by reaction of **1** with the substrate **2f**, the kinetic selectivity for the desired product **3f** over **5** exceeds 8/1. More likely **5** is produced to a significant extent through a slow cross-metathesis equilibrium with the coproduct **4** accumulating during the reaction in a sealed NMR tube. Under thermodynamic control (24 °C, sealed NMR tube) instead the reaction of one equiv. of **1** with **2f** reaches equilibrium within < 2 h (Figure 1B). The position of the equilibrium is driven by the effectively irreversible formation of 1,2-diarylethyne **7** that is slow to undergo cross-metathesis at 24 °C and favors the formation of **5** over **3f**.

Table 1. ROAMP initiators **3a-g** accessed by cross-metathesis of **1** with substituted (3,3,3-trifluoroprop-1-yn-1-yl)benzenes **2a-g**.

X =	alkyne	*T* (°C)	Mo complex	Yield (%)[a]
$N(CH_3)_2$	**2a**	24	**3a**	48 (96)
OCH_3	**2b**	0 to 24	**3b**	66 (94)
CH_3	**2c**	–20 to 24	**3c**	83 (95)
H	**2d**	–20 to 24	**3d**	79
OAc	**2e**	–60 to 24	**3e**	77 (92)
CF_3	**2f**	–60 to 24	**3f**	74 (92)
NO_2	**2g**	–60 to 24	**3g**	45 (83)

[a] Isolated yield after recrystallization. Crude NMR yields in parentheses.

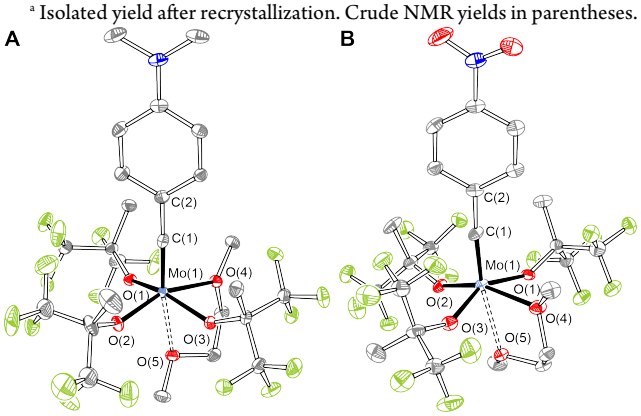

Figure 2. Single crystal X-ray structures of A) **3a** and B) **3g** exhibiting a meridional, pseudo-octahedral geometry at Mo. Thermal ellipsoids are drawn at the 50% probability level. Color coding: C (gray), O (red), F (green), Mo (turquoise). Hydrogen atoms are omitted for clarity.

Taking advantage of the regioselectivity inherent to the benzylidyne transfer with **2a-g** we prepared a series of ROAMP initiators featuring electron-donating ($N(CH_3)_2$, OCH_3, CH_3) and electron-withdrawing (OAc, CF_3, NO_2) substituents on the aromatic ring (Scheme 1). The precursor molybdenum propylidyne complex **1** can be synthesized on multi gram scale following a procedure pioneered by Gdula and Johnson.[38,67] The substituted carbyne transfer reagents **2a-g** are either commercially available or were prepared in 1–2 steps from simple starting materials. Addition of one equiv of **2a-g** to **1** in toluene at –60 to 24 °C and warming to 24 °C under dynamic vacuum (0.1 torr to remove volatile **4**) leads to the desired benzylidyne complexes **3a-g** in up to 96% crude yield (NMR), or 45–83% isolated yield following recrystallization (Table 1). A slight decrease in selectivity (96–83%) is observed as the polarization of the alkyne is altered by going from electron-donating **2a-c** to electron withdrawing substituents **2e-g** on the aromatic ring. If the trifluoromethyl group in **2a-g** is replaced by a methyl group the regioselectivity for the formation of **3a-g** falls below 70% (Supporting Information Figure S1). The reaction tolerates nucleophilic, electrophilic, basic, and potentially coordinating functional groups on the carbyne transfer reagent that are otherwise incompatible with the traditional low oxidation state route toward molybdenum benzylidyne complexes (Scheme 1).

NMR spectroscopy indicates that the molybdenum benzylidyne complexes **3a-g** prepared in this series are isostructural in solution. The structural homology is further supported by the crystallographic analysis of complexes **3a** and **3g** depicted in Figure 2. Dark green plates of **3a** from Et_2O/pentane (1:1) and orange prisms of **3g** from toluene/pentane (1:1) suitable for X-ray crystallography were obtained from saturated solutions at –35 °C. In both complexes the geometry at the Mo center is pseudo-octahedral. X-ray crystallography of **3a** (Figure 2A) confirms the presence of a C(1)≡Mo(1) triple bond with a bond length of 1.761(3) Å and a C(2)–C(1)–Mo(1) angle of 177.3(2)°. Three hexafluoro-*tert*-butoxide ligands adopt a meridional conformation featuring Mo(1)–O(1), Mo(1)–O(2), and Mo(1)–O(3) distances of 1.968(2) Å, 1.928(2) Å, and 1.975(2) Å. One equiv of DME is coordinated to the Mo complex in the crystal. The bond distances are 2.226(2) Å and 2.415(2) Å for the Mo(1)–O(4) *cis* and Mo(1)–O(5) *trans* to the carbyne, respectively. X-ray crystallography of **3g** (Figure 2B) shows that substitution of the electron donating $N(CH_3)_2$ group in **3a** for an electron withdrawing NO_2 group in **3g** has only a small effect on the C(1)≡Mo(1) bond length (1.754(7) Å) and C(2)–C(1)–Mo(1) bond angle (174.8(6)°). More pronounced changes are observed for the bond lengths between the molybdenum and the three hexafluoro-*tert*-butoxide ligands. The weaker π-donating character of the carbyne in **3g** is partially compensated by a contraction of the Mo(1)–O(1), Mo(1)–O(2), and Mo(1)–O(3) bond lengths, 1.958(4) Å, 1.922(4) Å, and 1.952(5) Å respectively.

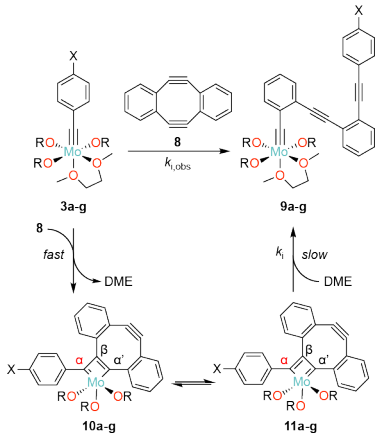

Scheme 2. Schematic representation of the ROAMP initiation step of substituted molybdenum benzylidyne complexes **3a-g** with ring-strained alkyne **8**. R = $CCH_3(CF_3)_2$

With a series of substituted ROAMP initiators **3a-g** in hand we explored the electronic effects on the ROAMP initiation step in the ring-opening metathesis of 5,6,11,12-tetradehydrobenzo[*a*,*e*][8]annulene (**8**). Upon addition of **8** to a twofold excess of **3a-g**, the ring-strained monomer is consumed in less than 60 s to yield a mixture of interconverting metallacyclobutadienes **10a-g** and **11a-g** (Scheme 2).[38] By ^{19}F and ^{1}H NMR we observe that the intermediate metallacyclobutadienes decay in a unimolecular process to give the ring-opened benzylidynes **9a-g**

(Figure 3A). As the initial cycloaddition between **3a**-**g** and **8** is almost instantaneous, the observed rate of initiation, $k_{i,obs}$ can be approximated by the rate limiting step, k_i. Fitting the experimental data to a first-order exponential decay of **10a**-**g** and **11a**-**g** gives a unique rate constant k_i for the cycloelimination step for each of the ROAMP initiators. As the isosteric series **3a**-**g** spans the Hammett parameter space, a linear free-energy relationship (LFER) analysis provides further insight into the structure of the rate determining transition state (Figure 3B). A positive Hammett reaction constant ρ = +0.36 is indicative of either the buildup of negative charge or the decrease of positive charge in the benzylic α-position in the rate determining transition state. The significant rate acceleration of the ROAMP initiation step upon introducing electron withdrawing groups on the benzylidyne complex is unusual and has not been observed for the analogous ring-opening metathesis polymerization (ROMP) with Mo or Ru carbene complexes.[68] This contrast is likely attributed to contributions from the extended π-conjugation of the metallacyclobutadiene that mediates resonance stabilization effects more efficiently than a saturated metallacyclobutane.

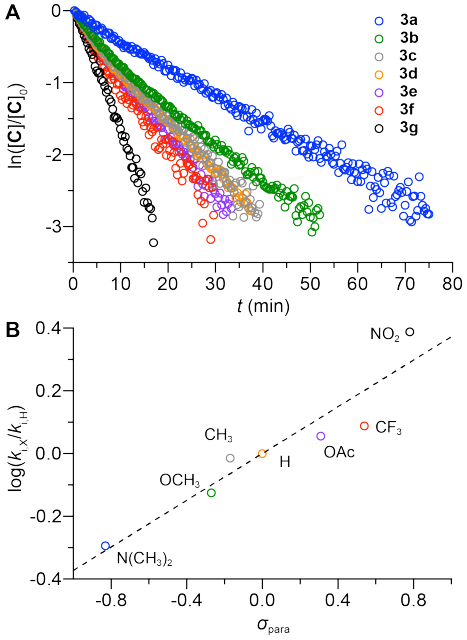

Figure 3. A) First-order kinetic plot of the rate-limiting ring-opening cycloelimination of **3a**-**g** with **8**. B) Hammett LFER analysis of the rate of initiation $k_{i,X}$ for **3a**-**g** with **8**.

To further support our interpretation of the LFER analysis, we used theory to explore the potential energy surface associated with the ROAMP initiation reaction. Figure 4 summarizes the results of density functional theory (DFT) calculations on three model complexes representative for the tetracoordinate Mo complexes resulting from the reversible dissociation of DME from **3a**, **3d**, or **3f** (equilibria involving reversible association of DME were not included in an effort to facilitate convergence on a flat potential energy surface). The coordination of ring-strained monomer **8** to the tetracoordinate complex **SM** is an exothermic process (–24 kcal mol^{-1}) and leads to intermediate **Int1**. A nearly barrierless cycloaddition step (**TS1**, for X = H) yields the initial metallacyclobutadiene intermediate **Int2** that is localized on a rather flat potential energy surface. **Int2** undergoes a double bond isomerization to give the secondary molybdacyclobutadiene **Int3**. While ^{19}F NMR spectroscopy clearly indicates an equilibrium between interconverting metallacyclobutadienes **10a**-**g** and **11a**-**g**, the barrier is only 1.5 kcal mol^{-1} by DFT gas phase calculations. The rate determining step in the ROAMP initiation is associated with the cycloelimination leading from **Int3** through **TS3** to the product **P**. While theory underestimates the magnitude of the barriers, the relative trends **TS3**(X = N(CH$_3$)$_2$) > **TS3**(X = H) > **TS3**(X = CF$_3$) faithfully reproduce the experimental results. Natural population analysis (NPA)[69] for X = H shows a buildup of negative charge at the benzylic α-position consistent with our Hammett LFER analysis. The charge decreases from +0.21 on the carbyne carbon atom in **Int1** to +0.14 in **TS1**, +0.07 in **Int2**, +0.11 in **TS2**, +0.03 in **Int3**, and finally –0.01 in the rate-limiting transition state **TS3**. As expected, electron donating substituents (X = N(CH$_3$)$_2$) lead to an increase of the activation barrier, while electron withdrawing groups (X = CF$_3$) stabilize the negative charge buildup in the transition state thereby lowering the energy of **TS3**.

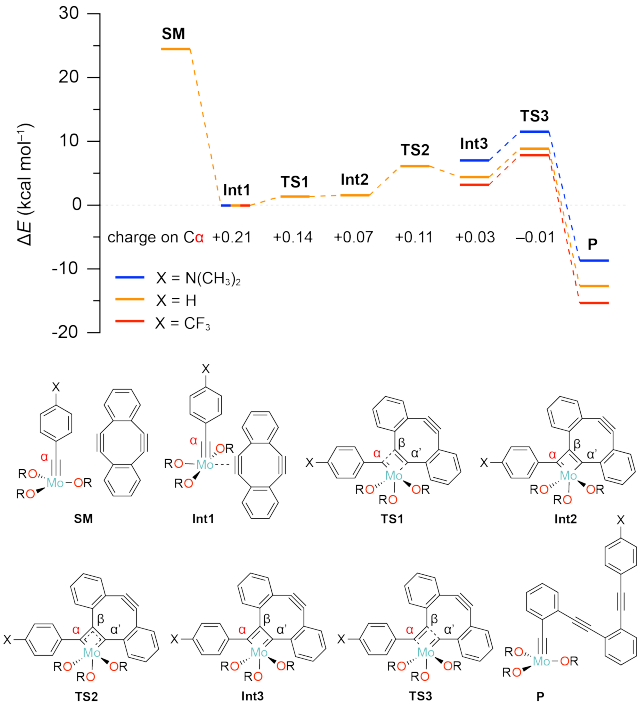

Figure 4. Calculated reaction coordinate diagram of the rate determining step in the ROAMP initiation reaction for three model complexes representing **3a** (X = N(CH$_3$)$_2$), **3d** (X = H), and **3f** (X = CF$_3$). (DFT ωB97xD; CHNOF (6-31G+(d,p)); Mo (SDD ECP MWB28); ZPE corrected) R = CCH$_3$(CF$_3$)$_2$

Table 2. Molecular weight analysis of *poly*-**8**

X =	[**8**]/[**3**]	M_n (SEC)[a]	M_w (SEC)[a]	$Đ_M$ (M_w/M_n)	cyclic *poly*-**8**
N(CH$_3$)$_2$	10/1	800	1700	2.1	60%
OCH$_3$	10/1	1800	3400	1.9	20%
CH$_3$	10/1	1900	3000	1.6	<1%[b]
H	10/1	1800	2500	1.4	<1%[b]
OAc	10/1	2500	3300	1.3	<1%[b]
CF$_3$	10/1	2600	3400	1.3	<1%[b]
NO$_2$	10/1	2600	3500	1.3	<1%[b]

[a] Size exclusion chromatography (SEC) calibrated to polystyrene standards. [b] Concentration below detection limit.

The observed rate acceleration attributed to the electronic stabilization of the cycloelimination transition state acts exclusively on the initiation step, k_i. The rate of propagation, k_p, for complexes **3a-g** is largely unaffected by substituent effects as the distance between the end group and the reaction center increases with each monomer in the growing polymer chain. Electron withdrawing substituents are thus uniquely suited to selectively increase k_i over k_p, a crucial requirement for the synthesis of living polymers with narrow molecular weight distributions. The effect is most apparent at high catalyst loadings (e.g. [**8**]/[**3a-g**] = 10/1, Table 2). The molecular weight dispersity, $Đ_M$,[70] of the resulting polymers derived from size-exclusion chromatography (SEC) ranges from 2.1 for electron donating X = $N(CH_3)_2$ to 1.3 for electron withdrawing substituents X = OAc, CF_3, NO_2. Polymers resulting from ROAMP initiators **3a** and **3b** feature an electron-rich activated alkyne as an end group that promotes intra- and intermolecular chain-transfer reactions. In fact, **3a** is even a superior catalyst for the synthesis of cyclic *poly*-**8** (as compared to **1**), yielding > 60% macrocyclic products in less than 2 h (Supporting Information Figures S2, S3). ROAMP initiators featuring electron-withdrawing groups instead deactivate the terminal alkyne preventing undesired chain-transfer processes that contribute to a broadening of the dispersity.

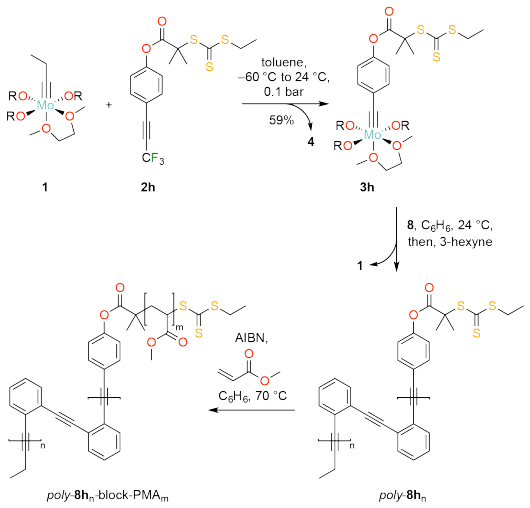

Scheme 3. Synthesis of telechelic ROAMP-RAFT copolymerization initiator via benzylidyne transfer to **3h**, followed by ROAMP of **8**, and RAFT chain-extension with methyl acrylate to give *poly*-**8h**-*block*-PMA. R = $CCH_3(CF_3)_2$

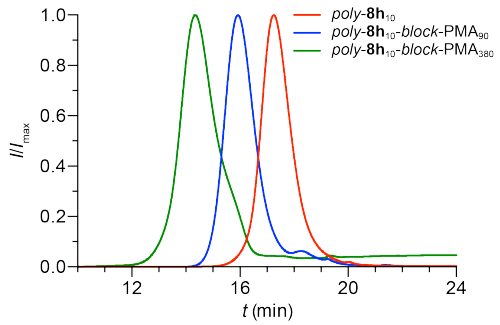

Figure 5. SEC traces showing the chain extension of macroinitiator *poly*-**8h** (red) to give *poly*-**8h**$_{10}$-*block*-PMA_{90} (blue) and *poly*-**8h**$_{10}$-*block*-PMA_{380} (green); calibrated to polystyrene standards.

Besides the obvious mechanistic advantages provided by electron withdrawing substituents in a controlled living ROAMP ($k_i > k_p$), the versatile and mild carbyne transfer reaction with readily accessible (3,3,3-trifluoroprop-1-yn-1-yl)benzenes described above gives access to telechelic polymers. Electron-withdrawing substituents such as the acyloxybenzylidyne **3e** (Scheme 1) provide a versatile functional group that serves as an adaptable chemical linker for post-polymerization functionalization. To further illustrate this concept, we synthesized (3,3,3-trifluoroprop-1-yn-1-yl)benzene **2h** featuring a trithiocarbonate group that acts as a reversible addition-fragmentation chain-transfer (RAFT) initiator (Scheme 3).[39,71] Benzylidyne transfer from **2h** cleanly yields the functionalized Mo complex **3h** in 59% isolated yield (86% by crude NMR). ROAMP of **8** with functional initiator **3h** followed by chain-termination with excess 3-hexyne yields *poly*-(*o*-phenylene ethynylene) *poly*-**8h**$_{10}$. The MALDI mass spectrum shows two families of molecular ions separated by the mass of the monomer **8** (MW = 200 g mol^{-1}) that correspond to linear polymers, functionalized with a fragment of the trithiocarbonate initiator on one end and a butyne group on the other (Supporting Information Figure S4). *Poly*-**8h**$_{10}$ acts as a functional macroinitiator for RAFT polymerization. Chain extension with methyl acrylate initiated by AIBN in benzene at 70 °C gives *poly*-(methyl acrylate) (PMA) block polymers *poly*-**8h**-*block*-PMA. The amphiphilic block copolymer can be isolated from a small amounts of PMA homopolymer either by precipitation in ethanol, Soxhlet extraction with acetonitrile, or by preparative SEC depending on the weight of the PMA block. The molecular weight increases from 2.5 kDa for *poly*-**8h**$_{10}$, to 9.6 kDa (corresponding to *poly*-**8h**$_{10}$-block-PMA_{90} by ^{1}H NMR end group analysis) without a significant broadening of the $Đ_M$ = 1.3. While block-copolymers featuring molecular weights up to 36 kDa, *poly*-**8h**$_{10}$-block-PMA_{380}, could be prepared by this method a challenging purification of block copolymers from PMA homopolymers resulting from radical chain-transfer processes leads to a slight broadening of the molecular weight distribution ($Đ_M$ = 1.5).

CONCLUSION

We herein report a novel highly regioselective carbyne transfer protocol that gives access to a large number of structurally diverse ROAMP initiators featuring both electrophilic and nucleophilic functional groups that are incompatible with traditional low oxidation state routes. Detailed kinetic analysis and Hammett linear free energy relationships reveal that electron withdrawing substituents on the benzylidyne effectively increase the rate of initiation k_i over the rate of propagation k_p. These kinetic studies are further corroborated by gas phase theoretical calculations that highlight a buildup of negative charge at the carbyne carbon atom in the rate determining cycloelimination step. Our regioselective functional group tolerant carbyne transfer strategy along with an expanded mechanistic insight have enabled the design of a bifunctional ROAMP-RAFT initiator complex that provides access to hybrid *poly*-(*o*-phenylene ethynylene)-*block*-*poly*-(methyl acrylate) block copolymers through a sequential ROAMP-RAFT polymerization protocol.

EXPERIMENTAL SECTION

Materials and General Methods. Unless otherwise stated, all manipulations of air and/or moisture sensitive compounds were carried out in oven-dried glassware, under an atmosphere of Ar or N_2. All solvents and reagents were purchased from Alfa Aesar, Spectrum Chemicals, Acros Organics, TCI America, Matrix Scientific, and Sigma-Aldrich and were used as received unless otherwise noted. Organic solvents were dried by passing through a column of alumina and were degassed by vigorous bubbling of N_2 or Ar through the solvent for 20 min. Liquid alkynes were dried over 4 Å molecular sieves. Commercial methyl acrylate was purified by extraction

with aqueous KOH and dried by passing through a column of alumina. Flash column chromatography was performed on SiliCycle silica gel (particle size 40–63 μm). Thin layer chromatography was performed using SiliCycle silica gel 60 Å F-254 precoated plates (0.25 mm thick) and visualized by UV absorption. All ^{1}H, {^{1}H}^{13}C, and ^{19}F NMR spectra were recorded on Bruker AV-600, DRX-500, AV-500, and AVQ-400 spectrometers, and are referenced to residual solvent peaks ($CDCl_3$ ^{1}H NMR δ = 7.26 ppm, ^{13}C NMR δ = 77.16 ppm; C_6D_6 ^{1}H NMR δ = 7.16 ppm, ^{13}C NMR δ = 128.06 ppm;) or hexafluorobenzene (19F NMR δ = –162.90 ppm). High-resolution mass spectrometry (EI) was performed on an Autospec Premier (Waters) sector spectrometer in positive ionization mode. ESI mass spectrometry was performed on a Finnigan LTQFT (Thermo) spectrometer. MALDI mass spectrometry was performed on a Voyager-DE PRO (Applied Biosystems Voyager System 6322) in positive mode using a matrix of dithranol or dithranol/$AgNO_3$. Elemental analysis (CHN) was performed on a Perkin Elmer 2400 Series II combustion analyzer (values are given in %). Size-exclusion chromatography (SEC) was carried out on a LC/MS Agilent 1260 Infinity set up with one guard and two Agilent Polypore 300 × 7.5 mm columns at 35 °C. All SEC analyses were performed on a 0.2 mg/mL solution of polymer in chloroform. An injection volume of 25 μL and a flow rate of 1 mL/min were used. Calibration was based on polystyrene standards ranging from M_w = 100 to 4,068,981 Da. X-ray crystallography of **3a** and **3g** was performed on an APEX II QUAZAR, using a Microfocus Sealed Source (Incoatec IμS; Mo-Kα radiation), Kappa Geometry with DX (Bruker-AXS build) goniostat, a Bruker APEX II detector, QUAZAR multilayer mirrors as the radiation monochromator, and Oxford Cryostream 700 at 100 K. Crystallographic data were solved with SHELXT, refined with SHELXL-2014, visualized with ORTEP-32, and finalized with WinGX. **1**,[38,67] **2b**,[72] **2c**,[72,73] **2d**,[72,73] **2f**,[74] and **2g**[72] and **8**[75] were synthesized following literature procedures.

Preparation of [4-((CH$_3$)$_2$N)-(C$_6$H$_4$)C≡Mo(OC(CH$_3$)(CF$_3$)$_2$)$_3$(DME)] (3a). A 10 mL flask was charged under N_2 with **1** (77 mg, 0.1 mmol) in toluene (2 mL, [**1**] = 50 mM). **2a** (21 mg, 0.1 mmol) was added at 24 °C to the reaction mixture. The flask was immediately placed under dynamic vacuum (0.1 torr) and the reaction mixture stirred for 1 h at 24 °C. The solvent was removed in vacuum at 24 °C and the residue was recrystallized from pentane/toluene (3:1, 1.5 mL) at –30 °C to yield **3a** (41 mg, 0.048 mmol, 48%) as a dark crystalline solid. ^{1}H NMR (600 MHz, C_6D_6, 22 °C) δ = 7.12 (d, J = 9.0 Hz, 2H), 6.15 (d, J = 9.0 Hz, 2H), 3.32 (s, 6H), 3.10 (s, 4H), 2.37 (s, 6H), 1.96 (s, 9H) ppm; ^{13}C{^{1}H} NMR (151 MHz. C_6D_6, 22 °C) δ = 297.7, 150.2, 134.5, 132.1, 124.9 (q, $^{1}J_{CF}$ = 289 Hz), 110.8, 84.1 (m, $^{2}J_{CF}$ = 29 Hz), 71.6, 63.7, 39.3, 19.3 ppm; ^{19}F NMR (376 MHz, C_6D_6, 22 °C) δ = –76.71 ppm; HRMS (EI) m/z: [4-((CH$_3$)$_2$N)-(C$_6$H$_4$)C≡Mo(OC(CH$_3$)(CF$_3$)$_2$)$_3$]$^+$ calcd [$C_{21}H_{19}F_{18}MoNO_3$] 773.0132; found 773.0132; Anal. calcd for [4-((CH$_3$)$_2$N)-(C$_6$H$_4$)C≡Mo(OC(CH$_3$)(CF$_3$)$_2$)$_3$(DME)]: C, 34.86; H, 3.39; N, 1.63. Found: C, 35.23; H, 3.41; N, 1.63. Dark green plates suitable for X-ray diffraction were grown from saturated pentane/Et_2O (1:1) solution at –35 °C. **3a** crystallizes in the monoclinic space group P 2$_1$/n, a =14.3977(5) Å, b = 14.4686(6) Å, c = 15.8068(7) Å, β = 100.490(2)°, Z = 4, GOF on F^2 = 1.051, R indices (all data) R1 = 0.0426, wR2 = 0.1021.

Preparation of [4-(CH$_3$O)-(C$_6$H$_4$)C≡Mo(OC(CH$_3$)(CF$_3$)$_2$)$_3$(DME)] (3b). A 10 mL flask was charged under N_2 with **1** (77 mg, 0.1 mmol) in toluene (2 mL, [**1**] = 50 mM). The solution was cooled to 0 °C and **2b** (22 mg, 0.11 mmol) was added to the reaction mixture. The flask was immediately placed under dynamic vacuum (0.1 torr) and removed from the cooling bath to warm to 24 °C. The solvent was removed in vacuum at 24 °C and the residue was recrystallized from pentane/toluene (4:1, 1 mL) at –30 °C to yield **3b** (56 mg, 0.066 mmol, 66%) as a red crystalline solid. ^{1}H NMR (600 MHz, C_6D_6, 22 °C) δ = 7.07 (d, J = 8.8 Hz, 2H), 6.48 (d, J = 8.8 Hz, 2H), 3.28 (s, 6H), 3.17 (s, 3H), 3.08 (s, 4H), 1.87 (s, 9H) ppm; ^{13}C{^{1}H} NMR (151 MHz. C_6D_6, 22 °C) δ = 295.3, 160.5, 137.9, 132.3, 124.8 (q, $^{1}J_{CF}$ = 290 Hz), 113.7, 84.1 (m, $^{2}J_{CF}$ = 29 Hz), 63.8, 54.9, 19.2 ppm; ^{19}F NMR (470 MHz, C_6D_6, 22 °C) δ = –76.68 ppm; HRMS (EI) m/z: [4-(CH$_3$O)-(C$_6$H$_4$)C≡Mo(OC(CH$_3$)(CF$_3$)$_2$)$_3$]$^+$ calcd [$C_{20}H_{16}F_{18}MoO_4$] 759.9815; found 759.9830; Anal. calcd for [4-((CH$_3$O)-(C$_6$H$_4$)C≡Mo(OC(CH$_3$)(CF$_3$)$_2$)$_3$(DME)]: C, 33.98; H, 3.09. Found: C, 34.27; H, 3.04.

Preparation of [4-CH$_3$-(C$_6$H$_4$)C≡Mo(OC(CH$_3$)(CF$_3$)$_2$)$_3$(DME)] (3c). A 10 mL flask was charged under N_2 with **1** (77 mg, 0.1 mmol) in toluene (2 mL, [**1**] = 50 mM). The solution was cooled to –20 °C and **2c** (22 mg, 0.11 mmol) was added to the reaction mixture. The flask was immediately placed under dynamic vacuum (0.1 torr) and removed from the cooling bath to warm to 24 °C. The solvent was removed in vacuum at 24 °C and the residue was recrystallized from pentane/Et_2O (4:1, 1 mL) at –30 °C to yield **3c** (69 mg, 0.083 mmol, 83%) as an orange crystalline solid. ^{1}H NMR (500 MHz, C_6D_6, 22 °C) δ = 7.05 (d, J = 8.0 Hz, 2H), 6.76 (d, J = 8.0 Hz, 2H), 3.29 (s, 6H), 3.06 (s, 4H), 2.03 (s, 3H), 1.84 (s, 9H) ppm; ^{19}F NMR (376 MHz, C_6D_6, 22 °C) δ = –76.85 ppm; HRMS (EI) m/z: [4-CH$_3$-(C$_6$H$_4$)C≡Mo(OC(CH$_3$)(CF$_3$)$_2$)$_3$]$^+$ calcd [$C_{20}H_{16}F_{18}MoO_3$] 743.9866; found 743.9854. Spectroscopic data is consistent with previous reports.[76]

Preparation of PhC≡Mo(OC(CH$_3$)(CF$_3$)$_2$)$_3$(DME)] (3d). A 10 mL flask was charged under N_2 with **1** (77 mg, 0.1 mmol) in toluene (2 mL, [**1**] = 50 mM). The solution was cooled to –20 °C and **2d** (34 mg, 0.2 mmol, 2 equiv due to its high volatility) was added to the reaction mixture. The flask was immediately placed under dynamic vacuum (0.1 torr) and removed from the cooling bath to warm to 24 °C. The solvent was removed in vacuum at 24 °C and the residue was recrystallized from pentane/Et_2O (1:1, 2 mL) at –30 °C to yield **3d** (65 mg, 0.079 mmol, 79%) as a red-orange crystalline solid. ^{1}H NMR (400 MHz, C_6D_6, 22 °C) δ = 7.11 (d, J = 7.4 Hz, 2H), 6.96 (t, J = 7.9 Hz, 2H), 6.75 (t, J = 7.5 Hz, 1H), 3.25 (s, 6H), 3.03 (s, 4H), 1.81 (s, 9H) ppm; ^{19}F NMR (376 MHz, C_6D_6, 22 °C) δ = –76.67 ppm; HRMS (EI) m/z: [(C$_6$H$_5$)C≡Mo(OC(CH$_3$)(CF$_3$)$_2$)$_3$]$^+$ calcd [$C_{19}H_{14}F_{18}MoO_3$] 729.9710; found 729.9722. Spectroscopic data is consistent with previous reports.[66]

Preparation of [4-(AcO)-(C$_6$H$_4$)C≡Mo(OC(CH$_3$)(CF$_3$)$_2$)$_3$(DME)] (3e). A 10 mL flask was charged under N_2 with **1** (77 mg, 0.1 mmol) in toluene (2 mL, [**1**] = 50 mM). The solution was cooled to –60 °C and **2e** (23 mg, 0.1 mmol) was added to the reaction mixture. The flask was immediately placed under dynamic vacuum (0.1 torr) and removed from the cooling bath to warm to 24 °C. The solvent was removed in vacuum at 24 °C and the residue was recrystallized from pentane/Et_2O (4:1, 1.5 mL) at –30 °C to yield **3e** (67 mg, 0.077 mmol, 77%) as a dark red crystalline solid. ^{1}H NMR (400 MHz, C_6D_6, 22 °C) δ = 7.12 (d, J = 8.7 Hz, 2H), 6.92 (d, J = 8.7 Hz, 2H), 3.24 (s, 6H), 3.06 (s, 4H), 1.79 (s, 9H), 1.70 (s, 3H) ppm; ^{13}C{^{1}H} NMR (126 MHz. C_6D_6, 22 °C) δ = 293.17, 168.3, 151.7, 141.1, 124.7 (q, $^{1}J_{CF}$ = 290 Hz), 121.6, 84.0 (m, $^{2}J_{CF}$ = 29 Hz), 71.6, 63.6, 20.4, 19.0 ppm; ^{19}F NMR (376 MHz, C_6D_6, 22 °C) δ = –76.70 ppm; HRMS (EI) m/z: [4-AcO-(C$_6$H$_4$)C≡Mo(OC(CH$_3$)(CF$_3$)$_2$)$_3$]$^+$ calcd [$C_{21}H_{16}F_{18}MoO_5$] 787.9764; found 787.9765; Anal. calcd for [4-AcO-(C$_6$H$_4$)C≡Mo(OC(CH$_3$)(CF$_3$)$_2$)$_3$(DME)]: C, 34.26; H, 2.99. Found: C, 34.59; H, 3.34.

Preparation of [4-CF$_3$-(C$_6$H$_4$)C≡Mo(OC(CH$_3$)(CF$_3$)$_2$)$_3$(DME)] (3f). A 20 mL flask was charged under N_2 with **1** (231 mg, 0.3 mmol) in toluene (6 mL, [**1**] = 50 mM). The solution was cooled to –60 °C and **2f** (87 mg, 0.36 mmol, 1.2 equiv) was added to the reaction mixture. The flask was immediately placed under dynamic vacuum (0.1 torr) and removed from the cooling bath to warm to 24 °C. The solvent was removed in vacuum at 24 °C and the residue was recrystallized from toluene (3 mL) at –25 °C and washed with cold pentane/Et_2O (1:1, 1 mL) to yield **3f** (196 mg, 0.22 mmol, 74%) as an orange crystalline solid. ^{1}H NMR (600 MHz, C_6D_6, 22 °C) δ = 7.12 (d, J = 8.2 Hz, 2H), 6.95 (d, J = 8.2 Hz, 2H), 3.22 (s, 6H), 3.03 (s, 4H), 1.73 (s, 9H) ppm; ^{13}C{^{1}H} NMR (126 MHz. $CDCl_3$, 22 °C) δ = 291.8, 145.3, 130.7 (q, $^{2}J_{CF}$ = 33 Hz), 130.3, 125.5 (q, $^{3}J_{CF}$ = 3.7 Hz), 123.9 (q, $^{1}J_{CF}$ = 289 Hz), 123.4 (q, $^{1}J_{CF}$ = 272 Hz), 83.7 (m, $^{2}J_{CF}$ = 29 Hz), 72.0, 64.0, 19.0 ppm; ^{19}F NMR (564 MHz, C_6D_6, 22 °C) δ = –62.71, –76.63 ppm; HRMS (EI) m/z: [4-CF$_3$-(C$_6$H$_4$)C≡Mo(OC(CH$_3$)(CF$_3$)$_2$)$_3$]$^+$ calcd [$C_{20}H_{13}F_{21}MoO_3$] 797.9583; found 797.9583; Anal. calcd for [4-CF$_3$-(C$_6$H$_4$)C≡Mo(OC(CH$_3$)(CF$_3$)$_2$)$_3$(DME)]: C, 32.52; H, 2.62. Found: C, 32.39; H, 2.73.

Preparation of [4-O$_2$N-(C$_6$H$_4$)C≡Mo(OC(CH$_3$)(CF$_3$)$_2$)$_3$(DME)] (3g). A 10 mL flask was charged under N_2 with **1** (154 mg, 0.2 mmol) in

toluene (4 mL, [**1**] = 50 mM). The solution was cooled to –60 °C and **2g** (44 mg, 0.2 mmol) was added to the reaction mixture. The flask was immediately placed under dynamic vacuum (0.1 torr) and removed from the cooling bath to warm to 24 °C. The solvent was removed in vacuum at 24 °C and the residue was recrystallized from pentane/ Et_2O (1:1, 1 mL) at –30 °C to yield **3e** (77 mg, 0.89 mmol, 45%) as a dark red crystalline solid. ^{1}H NMR (500 MHz, C_6D_6, 22 °C) δ = 7.58 (d, J = 8.9 Hz, 2H), 6.79 (d, J = 8.9 Hz, 2H), 3.21 (s, 6H), 3.02 (s, 4H), 1.71 (s, 9H) ppm; ^{13}C{^{1}H} NMR (126 MHz. C_6D_6, 22 °C) δ = 290.5, 147.1, 146.3, 130.4, 124.6 (q, $^1J_{CF}$ = 290 Hz), 123.7, 84.0 (m, $^2J_{CF}$ = 29 Hz), 71.7, 64.4, 18.9 ppm; ^{19}F NMR (376 MHz, C_6D_6, 22 °C) δ = –76.69 ppm; HRMS (EI) m/z: [4-O_2N-(C_6H_4)C≡Mo(OC(CH_3)(CF_3)$_2$)$_3$]$^+$ calcd [$C_{19}H_{13}F_{18}MoNO_5$] 774.9560; found 774.9560; Anal. calcd for [4-O_2N-(C_6H_4)C≡Mo(OC(CH_3)(CF_3)$_2$)$_3$(DME)]: C, 32.00; H, 2.69; N, 1.62. Found: C, 32.25; H, 2.60; N, 1.55. Orange prisms (yellow in transmission) suitable for X-ray diffraction were grown from saturated pentane/toluene (1:1) solution at –35 °C. The compound crystallizes in the monoclinic space group P 2_1, a = 9.4048(5) Å, b = 9.2801(5) Å, c = 17.2135(9) Å, β = 98.630(3)°, Z = 2, GOF on F^2 = 0.994, R indices (all data) R1 = 0.0544, wR2 = 0.0820.

Preparation of [4-(O(C=O)C(CH_3)$_2$S(C=S)SCH_2CH_3)-(C_6H_4)C≡Mo(OC(CH_3)(CF_3)$_2$)$_3$(DME)] (3h). A 10 mL flask was charged under N_2 with **1** (154 mg, 0.2 mmol) in toluene (4 mL, [**1**] = 50 mM). The solution was cooled to –60 °C and **2h** (78 mg, 0.2 mmol) was added to the reaction mixture. The flask was immediately placed under dynamic vacuum (0.1 torr) and removed from the cooling bath to warm to 24 °C. The solvent was removed in vacuum at 24 °C. The solid residue was dissolved in minimum pentane and precipitated with perfluoromethylcyclohexane (10 mL) at 24 °C to yield **3e** (122 mg, 0.12 mmol, 59%) as an orange powder. ^{1}H NMR (600 MHz, C_6D_6, 22 °C) δ = 7.05 (a q, J = 8.9 Hz, 2H), 3.23 (s, 6H), 3.05 (s, 4H), 2.87 (q, J = 7.4 Hz, 2H), 1.76 (s, 9H), 1.60 (s, 6H), 0.84 (t, J = 7.4 Hz, 3H) ppm; ^{13}C{^{1}H} NMR (151 MHz. C_6D_6, 22 °C) δ = 293.7, 222.4, 171.3, 152.4, 141.6, 131.9, 125.0 (q, $^1J_{CF}$ = 289 Hz), 122.0, 84.4 (m, $^2J_{CF}$ = 29 Hz), 71.9, 64.2, 56.2, 31.8, 25.5, 19.4, 13.0; ^{19}F NMR (376 MHz, C_6D_6, 22 °C) δ = –76.70 ppm; FTMS (ESI-TOF) m/z: [4-(EtSCS_2C(CH_3)$_2$$CO_2$)-($C_6H_4$)C≡Mo(OC($CH_3$)($CF_3$)$_2$)$_3$+AcO]$^-$ calcd [$C_{28}H_{27}F_{18}MoO_7S_3$] 1010.9686; found 1010.9653.

General procedure for ring-opening metathesis polymerization. A 20 mL vial was charged under N_2 with **8** (0.01 g, 0.05 mmol) in toluene (1.5 mL). **3a**-**h** (5.0 μmol) in toluene (0.6 mL) was added and the mixture was stirred for 2 h at 24 °C. 3-hexyne (0.11 mL, 1 mmol) was added to the reaction mixture, stirred for 15 min, and diluted with MeOH (10 mL). The solid precipitate was isolated by filtration and washed with MeOH (30 mL) and hexanes (10 mL) to yield *poly*-**8a**-**h** as a brown solid.

Preparation of *poly*-8h-*block*-PMA$_{90}$. A J. Young tube was charged with *poly*-**8h** (9 mg, 4 μmol), methyl acrylate (35 mg, 0.4 mmol) and AIBN (0.2 mg, 1.2 μmol) in C_6D_6 (0.5 mL). The reaction mixture was degassed and heated to 70 °C for 16 h. The reaction mixture was cooled to –40 °C and diluted with EtOH (15 mL). The precipitate was washed with EtOH (5 mL), dried under vacuum, disolved in MeCN (4 mL), filtered (0.2 μm nylon membrane), and evaporated to yield *poly*-**8h**-*block*-PMA$_{90}$ (16 mg, 42%) as a brown solid. ^{1}H NMR (600 MHz, $CDCl_3$, 22 °C) δ = 7.50 (br, 40H), 7.15 (br, 40H), 3.66 (s, 270H), 3.37 (q, J = 7.4 Hz, 2H), 2.58 (br, 1 H), 2.33 (br, 90H), 1.93 (br, 30H), 1.69 (br, 90H), 1.60–1.41 (m, 60H), 1.40–1.19 (m, 119H) ppm; ^{13}C{^{1}H} NMR (151 MHz, $CDCl_3$, 22 °C) δ = 175.0, 132.2, 128.1, 125.7, 92.6, 51.8, 41.6–41.3 (m), 36.3–34.1(m) ppm.

Preparation of *poly*-8h-*block*-PMA$_{380}$. A J. Young tube was charged with *poly*-**8h** (6 mg, 2.5 μmol), methyl acrylate (475 mg, 0.5 mL, 5.5 mmol) and AIBN (80 μg, 0.5 μmol) in C_6D_6 (0.5 mL). The reaction mixture was degassed and heated to 70 °C for 3 h. The reaction mixture was cooled to –40 °C and diluted with EtOH (15 mL). The precipitate was washed with EtOH (5 mL), dried under vacuum. Preparative size exclusion chromatography (35 °C, $CHCl_3$) yielded *poly*-**8h**-*block*-PMA$_{380}$ (23 mg, 25%) as a brown solid. ^{1}H NMR (600 MHz, $CDCl_3$, 22 °C) δ = 7.49 (br, 46H), 7.35 (d, J = 7.3 Hz, 2H), 7.12 (br, 45H), 7.01 (d, J = 8.2 Hz, 2H), 3.64 (s, 1139H), 3.35 (q, J = 7.4 Hz, 2H), 2.56 (br, 1H), 2.30 (m, 378H), 1.91 (m, 172H), 1.78–1.60 (m, 398H), 1.48 (m, 183H) ppm; ^{13}C{^{1}H} NMR (151 MHz, $CDCl_3$, 22 °C) δ = 175.0, 132.2, 128.1, 125.7, 92.6, 51.8, 41.6–41.3 (m), 36.3–34.1(m) ppm.

ASSOCIATED CONTENT

Supporting Information

Figures S1 to S4, methods and instrumentation, synthetic procedures for **2a**, **2e**, and **2h** and characterization, kinetic experiments, computational details (Tables S1 to S2) and X-ray crystallographic data (Tables S3 to S12), and NMR spectra (Figures S7 to S37), are included in the Supporting Information. This material is available free of charge via the WWW at http://pubs.acs.org.

AUTHOR INFORMATION

Corresponding Author

* ffischer@berkeley.edu

Author Contributions

All authors approved the final version of the manuscript.

ACKNOWLEDGMENT

Research supported by the National Science Foundation under contract number CHE-1455289, Berkeley Molecular Graphics and Computation Facility is supported in part by NSF grant CHE-0840505, Berkeley NMR Facility is supported in part by NIH grant SRR023679A, and X-Ray Facility is supported in part by NIH Shared Instrumentation Grant S10-RR027172. The authors acknowledge Dr. Hasan Celik for support with NMR acquisition, Dr. Antonio DiPasquale for assistance with X-ray analysis, and Dr. Rita Nichiporuk for assistance with ESI-TOF.

REFERENCES

(1) Friend, R. H.; Gymer, R. W.; Holmes, A. B.; Burroughes, J. H.; Marks, R. N.; Taliani, C.; Bradley, D. D. C.; Santos, D. A. D.; Brédas, J. L.; Lögdlund, M.; Salaneck, W. R. *Nature* **1999**, *397*, 121–128.

(2) Grimsdale, A. C.; Leok Chan, K.; Martin, R. E.; Jokisz, P. G.; Holmes, A. B. *Chem. Rev.* **2009**, *109*, 897–1091.

(3) Reineke, S.; Lindner, F.; Schwartz, G.; Seidler, N.; Walzer, K.; Lüssem, B.; Leo, K. *Nature* **2009**, *459*, 234–238.

(4) Cheng, Y.-J.; Yang, S.-H.; Hsu, C.-S. *Chem. Rev.* **2009**, *109*, 5868–5923.

(5) Dou, L.; Liu, Y.; Hong, Z.; Li, G.; Yang, Y. *Chem. Rev.* **2015**, *115*, 12633–12665.

(6) Busby, E.; Xia, J.; Wu, Q.; Low, J. Z.; Song, R.; Miller, J. R.; Zhu, X.-Y.; Campos, L. M.; Sfeir, M. Y. *Nat. Mater.* **2015**, *14*, 426–433.

(7) Kim, G.; Kang, S.-J.; Dutta, G. K.; Han, Y.-K.; Shin, T. J.; Noh, Y.-Y.; Yang, C. *J. Am. Chem. Soc.* **2014**, *136*, 9477–9483.

(8) Oh, J. Y.; Rondeau-Gagné, S.; Chiu, Y.-C.; Chortos, A.; Lissel, F.; Wang, G.-J. N.; Schroeder, B. C.; Kurosawa, T.; Lopez, J.; Katsumata, T.; Xu, J.; Zhu, C.; Gu, X.; Bae, W.-G.; Kim, Y.; Jin, L.; Chung, J. W.; Tok, J. B.-H.; Bao, Z. *Nature* **2016**, *539*, 411–415.

(9) Jansen-van Vuuren, R. D.; Armin, A.; Pandey, A. K.; Burn, P. L.; Meredith, P. *Adv. Mater.* **2016**, *28*, 4766–4802.

(10) Rochat, S.; Swager, T. M. *ACS Appl. Mater. Interfaces* **2013**, *5*, 4488–4502.

(11) Cowan, S. R.; Banerji, N.; Leong, W. L.; Heeger, A. J. *Adv. Funct. Mater.* **2012**, *22*, 1116–1128.

(12) Noriega, R.; Rivnay, J.; Vandewal, K.; Koch, F. P. V.; Stingelin, N.; Smith, P.; Toney, M. F.; Salleo, A. *Nat. Mater.* **2013**, *12*, 1038–1044.

(13) Huang, H.; Chen, Z.; Ortiz, R. P.; Newman, C.; Usta, H.; Lou, S.; Youn, J.; Noh, Y.-Y.; Baeg, K.-J.; Chen, L. X.; Facchetti, A.; Marks, T. *J. Am. Chem. Soc.* **2012**, *134*, 10966–10973.

(14) Sirringhaus, H.; Wilson, R. J.; Friend, R. H. *Appl. Phys. Lett.* **2000**, *77*, 406–408.

(15) Jeong, K. S.; Pensack, R. D.; Asbury, J. B. *Acc. Chem. Res.* **2013**, *46*, 1538–1547.
(16) Remy, R.; Wei, S.; Campos, L. M.; Mackay, M. E. *ACS Macro Lett.* **2015**, *4*, 1051–1055.
(17) Lombeck, F.; Di, D.; Yang, L.; Meraldi, L.; Athanasopoulos, S.; Credgington, D.; Sommer, M.; Friend, R. H. *Macromolecules* **2016**, *49*, 9382–9387.
(18) D'Innocenzo, V.; Luzio, A.; Abdalla, H.; Fabiano, S.; A. Loi, M.; Natali, D.; Petrozza, A.; Kemerink, M.; Caironi, M. *J. Mater. Chem. C* **2016**, *4*, 11135–11142.
(19) R. McNeill, C. *Energy Environ. Sci.* **2012**, *5*, 5653–5667.
(20) Bartelt, J. A.; Beiley, Z. M.; Hoke, E. T.; Mateker, W. R.; Douglas, J. D.; Collins, B. A.; Tumbleston, J. R.; Graham, K. R.; Amassian, A.; Ade, H.; Fréchet, J. M. J.; Toney, M. F.; McGehee, M. D. *Adv. Energy Mater.* **2013**, *3*, 364–374.
(21) Tran, H.; Gopinadhan, M.; Majewski, P. W.; Shade, R.; Steffes, V.; Osuji, C. O.; Campos, L. M. *ACS Nano* **2013**, *7*, 5514–5521.
(22) Kang, H.; Lee, W.; Oh, J.; Kim, T.; Lee, C.; Kim, B. J. *Acc. Chem. Res.* **2016**, *49*, 2424–2434.
(23) Prince, R. B.; Saven, J. G.; Wolynes, P. G.; Moore, J. S. *J. Am. Chem. Soc.* **1999**, *121*, 3114–3121.
(24) Lahiri, S.; Thompson, J. L.; Moore, J. S. *J. Am. Chem. Soc.* **2000**, *122*, 11315–11319.
(25) Bunz, U. H. F. *Chem. Rev.* **2000**, *100*, 1605–1644.
(26) Kübel, C.; Mio, M. J.; Moore, J. S.; Martin, D. C. *J. Am. Chem. Soc.* **2002**, *124*, 8605–8610.
(27) Blatchly, R. A.; Tew, G. N. *J. Org. Chem.* **2003**, *68*, 8780–8785.
(28) Jones, T. V.; Slutsky, M. M.; Laos, R.; de Greef, T. F. A.; Tew, G. N. *J. Am. Chem. Soc.* **2005**, *127*, 17235–17240.
(29) Jones, T. V.; Slutsky, M. M.; Tew, G. N. *New J. Chem.* **2008**, *32*, 676–679.
(30) Ghosh, K.; Moore, J. S. *J. Am. Chem. Soc.* **2011**, *133*, 19650–19652.
(31) Kloppenburg, L.; Song, D.; Bunz, U. H. F. *J. Am. Chem. Soc.* **1998**, *120*, 7973–7974.
(32) Kloppenburg, L.; Jones, D.; Bunz, U. H. F. *Macromolecules* **1999**, *32*, 4194–4203.
(33) Zhang, W.; Moore, J. S. *J. Am. Chem. Soc.* **2005**, *127*, 11863–11870.
(34) Bunz, U. H. F. *Macromol. Rapid Commun.* **2009**, *30*, 772–805.
(35) Lysenko, S.; Haberlag, B.; Wu, X.; Tamm, M. *Macromol. Symp.* **2010**, *293*, 20–23.
(36) Hu, K.; Yang, H.; Zhang, W.; Qin, Y. *Chem. Sci.* **2013**, *4*, 3649–3653.
(37) Yang, H.; Jin, Y.; Du, Y.; Zhang, W. *J. Mater. Chem. A* **2014**, *2*, 5986–5993.
(38) von Kugelgen, S.; Bellone, D. E.; Cloke, R. R.; Perkins, W. S.; Fischer, F. R. *J. Am. Chem. Soc.* **2016**, *138*, 6234–6239.
(39) Chiefari, J.; Chong, Y. K. (Bill); Ercole, F.; Krstina, J.; Jeffery, J.; Le, T. P. T.; Mayadunne, R. T. A.; Meijs, G. F.; Moad, C. L.; Moad, G.; Rizzardo, E.; Thang, S. H. *Macromolecules* **1998**, *31*, 5559–5562.
(40) Fischer, E. O.; Maasböl, A. *Chem. Ber.* **1967**, *100*, 2445–2456.
(41) Fischer, E. O.; Kreis, G.; Kreiter, C. G.; Mülle, J.; Huttner, G.; Lorenz, H. *Angew. Chem.* **1973**, *85*, 618–620.
(42) McDermott, G. A.; Dorries, A. M.; Mayr, A. *Organometallics* **1987**, *6*, 925–931.
(43) Abernethy, R. J.; F.Hill, A.; Neumann, H.; Willis, A. C. *Inorganica Chim. Acta* **2005**, *358*, 1605–1613.
(44) Heppekausen, J.; Stade, R.; Kondoh, A.; Seidel, G.; Goddard, R.; Fürstner, A. *Chem. – Eur. J.* **2012**, *18*, 10281–10299.
(45) Haberlag, B.; Freytag, M.; Daniliuc, C. G.; Jones, P. G.; Tamm, M. *Angew. Chem. Int. Ed.* **2012**, *51*, 13019–13022.
(46) Lysenko, S.; Volbeda, J.; Jones, P. G.; Tamm, M. *Angew. Chem. Int. Ed.* **2012**, *51*, 6757–6761.
(47) Haberlag, B.; Freytag, M.; Jones, P. G.; Tamm, M. *Adv. Synth. Catal.* **2014**, *356*, 1255–1265.
(48) Strutz, H.; Schrock, R. R. *Organometallics* **1984**, *3*, 1600–1601.
(49) Blackwell, J. M.; Figueroa, J. S.; Stephens, F. H.; Cummins, C. C. *Organometallics* **2003**, *22*, 3351–3353.
(50) Geyer, A. M.; Holland, M. J.; Gdula, R. L.; Goodman, J. E.; Johnson, M. J. A.; Kampf, J. W. *J. Organomet. Chem.* **2012**, *708–709*, 1–9.
(51) Laplaza, C. E.; Odom, A. L.; Davis, W. M.; Cummins, C. C.; Protasiewicz, J. D. *J. Am. Chem. Soc.* **1995**, *117*, 4999–5000.
(52) Tsai, Y.-C.; Johnson, M. J. A.; Mindiola, D. J.; Cummins, C. C.; Klooster, W. T.; Koetzle, T. F. *J. Am. Chem. Soc.* **1999**, *121*, 10426–10427.
(53) Fürstner, A.; Mathes, C.; Lehmann, C. W. *J. Am. Chem. Soc.* **1999**, *121*, 9453–9454.
(54) Fürstner, A.; Mathes, C.; Lehmann, C. W. *Chem. – Eur. J.* **2001**, *7*, 5299–5317.
(55) Tsai, Y.-C.; Stephens, F. H.; Meyer, K.; Mendiratta, A.; Gheorghiu, M. D.; Cummins, C. C. *Organometallics* **2003**, *22*, 2902–2913.
(56) Zhang, W.; Kraft, S.; S. Moore, J. *Chem. Commun.* **2003**, 832–833.
(57) Zhang, W.; Kraft, S.; Moore, J. S. *J. Am. Chem. Soc.* **2004**, *126*, 329–335.
(58) Zhang, W.; Cho, H.-M.; Moore, J. S. *Org. Synth.* **2007**, *84*, 163.
(59) Jyothish, K.; Zhang, W. *Angew. Chem. Int. Ed.* **2011**, *50*, 8478–8480.
(60) Jyothish, K.; Zhang, W. *Angew. Chem. Int. Ed.* **2011**, *50*, 3435–3438.
(61) Sedbrook, D. F.; Paley, D. W.; Steigerwald, M. L.; Nuckolls, C.; Fischer, F. R. *Macromolecules* **2012**, *45*, 5040–5044.
(62) Yang, H.; Liu, Z.; Zhang, W. *Adv. Synth. Catal.* **2013**, *355*, 885–890.
(63) Schaubach, S.; Gebauer, K.; Ungeheuer, F.; Hoffmeister, L.; Ilg, M. K.; Wirtz, C.; Fürstner, A. *Chem. – Eur. J.* **2016**, *22*, 8494–8507.
(64) Du, Y.; Yang, H.; Zhu, C.; Ortiz, M.; Okochi, K. D.; Shoemaker, R.; Jin, Y.; Zhang, W. *Chem. – Eur. J.* **2016**, *22*, 7959–7963.
(65) Haberlag, B.; Wu, X.; Brandhorst, K.; Grunenberg, J.; Daniliuc, C. G.; Jones, P. G.; Tamm, M. *Chem. – Eur. J.* **2010**, *16*, 8868–8877.
(66) McCullough, L. G.; Schrock, R. R.; Dewan, J. C.; Murdzek, J. C. *J. Am. Chem. Soc.* **1985**, *107*, 5987–5998.
(67) Gdula, R. L.; Johnson, M. J. A. *J. Am. Chem. Soc.* **2006**, *128*, 9614–9615.
(68) Schwab, P.; Grubbs, R. H.; Ziller, J. W. *J. Am. Chem. Soc.* **1996**, *118*, 100–110.
(69) Reed, A. E.; Weinstock, R. B.; Weinhold, F. *J. Chem. Phys.* **1985**, *83*, 735–746.
(70) Stepto, R. F. T. *Pure Appl. Chem.* **2009**, *81*, 351–353.
(71) Mahanthappa, M. K.; Bates, F. S.; Hillmyer, M. A. *Macromolecules* **2005**, *38*, 7890–7894.
(72) Kobayashi, Y.; Yamashita, T.; Takahashi, K.; Kuroda, H.; Kumadaki, I. *Tetrahedron Lett.* **1982**, *23*, 343–344.
(73) Tresse, C.; Guissart, C.; Schweizer, S.; Bouhoute, Y.; Chany, A.-C.; Goddard, M.-L.; Blanchard, N.; Evano, G. *Adv. Synth. Catal.* **2014**, *356*, 2051–2060.
(74) Konno, T.; Chae, J.; Kanda, M.; Nagai, G.; Tamura, K.; Ishihara, T.; Yamanaka, H. *Tetrahedron* **2003**, *59*, 7571–7580.
(75) Orita, A.; Hasegawa, D.; Nakano, T.; Otera, J. *Chem. – Eur. J.* **2002**, *8*, 2000–2004.
(76) Bellone, D. E.; Bours, J.; Menke, E. H.; Fischer, F. R. *J. Am. Chem. Soc.* **2015**, *137*, 850–856.

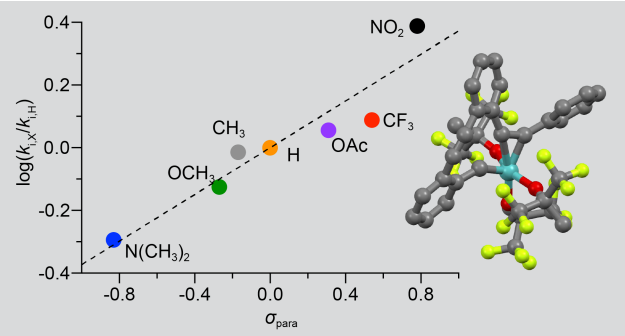
0.4
0.2
0.0
-0.2
-0.4
log(k1,X/k1,H)
NO2
CF3
CH3
H
OAc
OCH3
N(CH3)2
-0.8
-0.4
0.0
0.4
0.8
σpara